Journal of the European Ceramic Society 17 (1997) 1351–1359
© 1997 Elsevier Science Limited
Printed in Great Britain. All rights reserved
PII: S0955-2219(96)00242-7
0955-2219/97/$17.00

Microstructure, Strength and Fracture Characteristics of a Free-Standing Plasma-Sprayed Alumina

R. J. Damani[a] and E. H. Lutz[b]

[a]Institut für Struktur- und Funktionskeramik, Montanuniversität Leoben, Leoben, Austria
[b]LWK Plasmakeramik GmbH, Gummersbach, Germany

(Received 9 July 1996; revised version received 18 November 1996; accepted 25 November 1996)

Abstract

Plasma spraying, commonly used to apply wear and heat-resistant barriers, can be adapted to produce free-standing bulk ceramic parts. In this work the strength and fracture characteristics of a bulk plasma-sprayed alumina material with a highly aligned quasi-layered microstructure and about 14% porosity, are investigated for both the as-sprayed and annealed material conditions. It is found that strength and toughness for fracture normal to grain (splat) alignment are three times higher than for fracture parallel to the alignment. Subsequent annealing increases strength and toughness further by a factor of about three in both directions. The porosity change on annealing is low, despite a 9% volume shrinkage. Both material conditions exhibit pronounced R*-curve behaviour. The marked strength and fracture anisotropy is clearly a consequence of the pronounced alignment of microstructure itself, and the occurrence of a splat-internal microcrack sub-structure in the as-sprayed condition. The fracture path observed in the as-sprayed material is primarily transgranular (i.e. through the splats), and not along splat interfaces as previously reported for plasma-sprayed ceramics. © 1997 Elsevier Science Limited.*

1 Introduction

Plasma spraying, originally a surface coating technology used for applying wear- and heat-resistant barriers to metal and non-metal substrates, can be adapted to produce free-standing engineering ceramic parts such as plates and tubes of almost any size (metres in length and centimetres in thickness).[1–4] These materials exhibit thermo-mechanical properties which can differ quite strongly from the properties of ceramic materials produced by more conventional routes. Furthermore, since components can be produced directly with the desired dimensions, and the usual stages of green body formation and sintering are avoided, this approach can offer a real, efficient alternative to traditional manufacturing processes.[5]

Bulk plasma-sprayed ceramic materials exhibit porosity of between 5 and 20%, depending on the conditions of spraying, low elastic moduli compared to conventional materials (typically between 4 and 20 GPa), and flexural strengths of only 14 to 40 MPa.[6–8] The manufacturing process results in a characteristic layered structure consisting of aligned platelets ('splats'), high intergranular porosity, and pronounced microstructural anisotropy. As a consequence of the unique microstructure and special mechanical properties these materials are less prone to catastrophic brittle failure and it is possible to machine and finish components by conventional and novel means, e.g. laser and water-jet cutting as well as grinding, milling and drilling. They are also capable of withstanding very steep thermal gradients, i.e. they possess a much higher thermal shock resistance than comparable porous engineering ceramics. For example, a plasma-sprayed alumina when water-quenched may withstand a temperature change of up to 1000°C without any appreciable deterioration in residual strength.[7, 10–12].

Subsequent heat treatments (annealing) of as-sprayed materials can lead to substantial increases in elastic modulus and strength. Associated with this is a relatively low amount of shrinkage (about 2 to 3% linear shrinkage) and a related density increase.[6,7] However, it has been observed that such treatments result in a significant reduction in thermal shock resistance.

Until recently most research on the fracture of plasma-sprayed materials has been carried out on thin coatings or on substrate near layers. It is the

purpose of this work to investigate the strength and fracture characteristics of a bulk plasma-sprayed alumina material, in both the as-sprayed and annealed conditions, and to relate the observed phenomena to the phase and microstructural development of the material.

2 Experimental Procedure

2.1 Material

An alumina powder agglomerate (CT 100, Alcoa Chemie GmbH, Ludwigshafen, Germany, composition: α-Al_2O_3 99·50%, with additions of Na_2O, SiO_2, CaO, and Fe_2O_3, median powder agglomerate size 92·7 μm with 86% over 63 μm) was used for the production of a thick hollow cylinder of 275 mm outer and 119 mm inner diameters. The individual crystallites that formed the agglomerate were between 2 and 5 μm in diameter. The material was atmospheric plasma spray (APS) deposited by LWK Plasmakeramik, Gummersbach, Germany, in several passes using a water-stabilized arc plasma gun, onto a reusable steel mandrel, which was later removed by cold contraction.

2.2 Mechanical and physical testing

An 8-mm thick disc was cut from the cylinder and ground on both sides to a final thickness of 5 mm. One side was polished and four compact tension (CT) and 12 three-point bend test specimens were cut out. The specimens were all pre-notched by laser beam and the notches were manually extended and sharpened by use of a razor blade. The positions of the samples in the disc and the orientation of the notches are shown in Fig. 1. Specimens 2–4, 8–10 and 14–16 were annealed in air at 1550°C for 4 h.

In a first mechanical test sequence the fracture toughness of samples 5–10 and 11–16 was determined in three-point bending. The initial sharpened notch depth, a_0, to sample width, W ratio varied between 0·46 and 0·49. The outer span of the bending fixture was 69 mm. The samples were loaded to fracture with the cross-head speed of 1 mm/min. The fracture toughness, K_{Ic} is calculated from

$$K_{Ic} = Y \sigma \sqrt{a} , \quad (1)$$

where σ is the outer fibre stress calculated using the load at fracture, a is the length of the crack at fracture and Y is a geometric correction factor dependent on the crack length to sample width ratio, a/W, as given in Ref. 13.

The fractured halves of the first test sequence were used to prepare a further 24 three-point bending flexural strength test samples. These were tested in flat support (i.e. with the 5 mm dimension as height) and with 32 mm outer roll span and 0·3 mm/min cross-head speed.

R-curve experiments were performed using the four CT-specimens shown in Fig. 1. The initial notch depth to sample width ratio, a_0/W, was 0·51 for all samples. The specimens were carefully

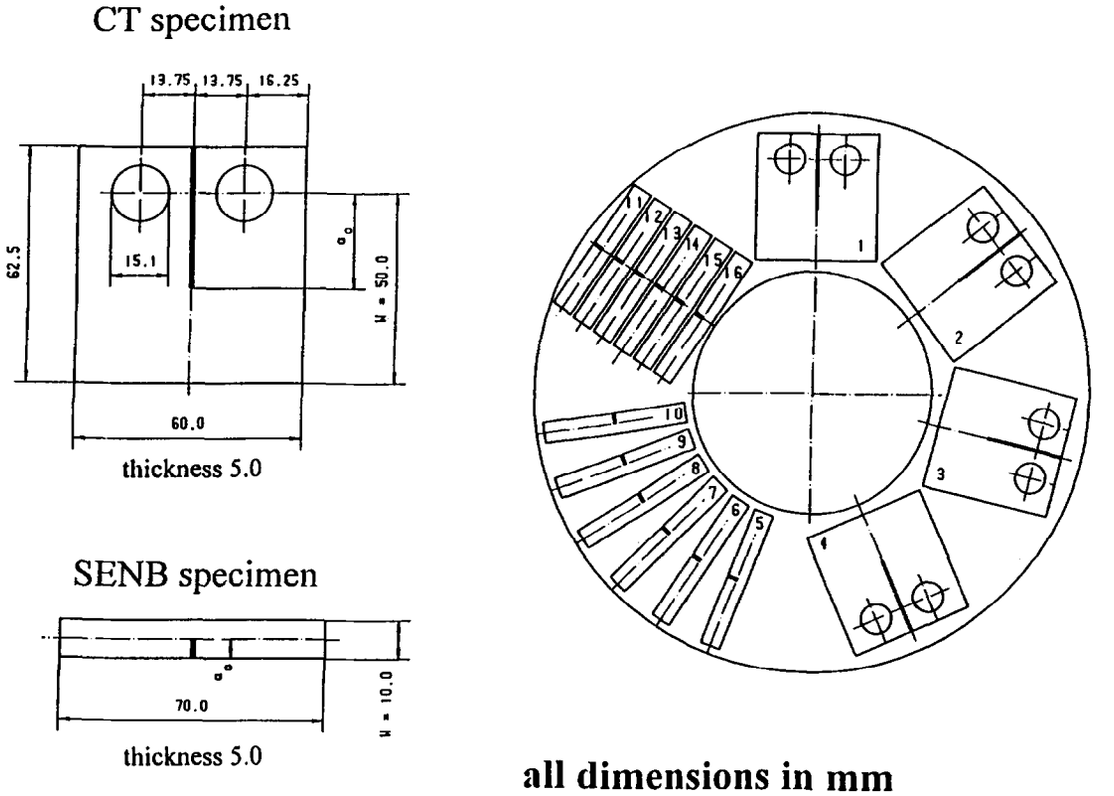

Fig. 1. Sample geometry and arrangement in the disc of plasma-sprayed alumina.

loaded in cycles with a cross-head speed of 0·1 mm/min. Crack extension was measured directly using a travelling optical microscope. The K_R values were calculated from

$$K_R = Y \frac{P}{b\sqrt{W}}, \quad (2)$$

where P is the load, b is the sample thickness. The appropriate value of the geometric correction factor Y (valid for $a/W < 0{\cdot}85$) is given by the relationship in Ref. 14.

The densities of the as-sprayed and annealed materials were determined on the basis of the weights and dimensions of fractured halves of samples 5–16; six samples were used for each material condition.

2.3 Microscopy and phase analyses

Microstructural and fracture path/fracture surface analyses were carried out on an annealed CT-sample and on an as-sprayed CT-sample, both optically and by using a scanning electron microscope (Cambridge stereoscan 360 equipped with microspec WDX 3PC). Section preparation was done using the standard techniques of embedding, grinding and polishing suitably oriented material. The samples, especially those of the as-sprayed material, proved to be very pressure and speed sensitive. As a result many sections were rendered unusable due to excessive breakout. In general, standard preparation techniques were found to be adequate, but tedious.

Phase and texture analysis was carried by X-ray diffraction on small coupons of bulk material. A Siemens D500 diffractometer with Cu K_α radiation (λ = 1·542 Å) in line focus and with a Ni filter was used for phase determination. Phase and pole-figure analyses were also performed using a Seifert C3000 diffractometer in spot focus and a V-filter with Cr K_α radiation (λ = 2·291 Å). The (116) and (400) pole axes were used for α-alumina and γ-alumina respectively.

3 Results

3.1 Microstructural analysis

The microstructure of the plasma-sprayed material can be seen in the micrographs in Figs 2(a) and 2(b). It clearly consists of platelets that are layered on top of each other to form a highly aligned quasi-layered structure. The micrographs show the microstructure of a radial section through the cylinder, i.e. a cross-section through the thickness of the material. A lot of open splat interfaces and boundaries may be observed, and there is obviously a lot of mechanical interlocking. A number of spherical grains embedded in this layered structure were also observed during the analysis. However, these are not evident in the micrographs presented. These were probably alumina powder particles that were not completely melted on spraying. The one striking feature of the as-sprayed material is the amount of fine, splat-internal, cracking (Fig. 2(b)). These fine cracks run normal to the splat surface through the entire thickness of the platelets. They are to a great extent aligned parallel to the direction of spraying. It is not clear whether these cracks were initially present in the bulk material, or if they were first introduced during sample preparation. If they are a result of the preparation process, their orientation indicates propagation along weak interfaces. The splats are about 10 μm thick through their centre and are on average about 100 μm in their long axis.

The overall microstructure of the annealed material is surprisingly similar to that of the as-sprayed material. The splats are marginally larger; they are in average about 15 μm through their centres and 110 μm in the long axis (see Fig. 3). The overall degree of porosity seems to be

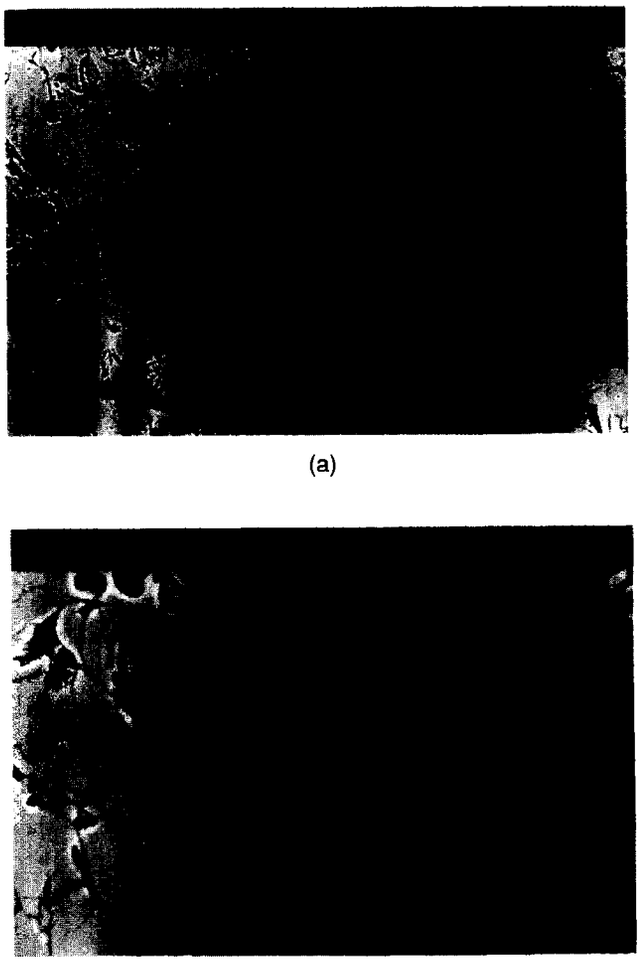

(a)

(b)

Fig. 2. Microstructure of the as-sprayed material: (a) showing the layered structure and inter-splat porosity, (b) magnified to show the splat-internal cracking.

Fig. 3. Microstructure of the annealed material magnified to show the changes in splat-internal cracking.

virtually the same as in the as-sprayed condition. The most obvious difference is that many of the finer cracks and boundaries have begun to heal, hence the nominal increase in splat size. Most splat-internal cracks no longer extend through the entire thickness of the platelets. There appears to be an increase in fine splat-internal spherical porosity. There is also less break-out in the polished annealed sample than in the comparable as-sprayed sample.

It is worth noting that a sintered alumina from a similar starting powder might be expected to contain some secondary, glassy, phase at grain boundaries and triple points.[15] Although this glassy phase is known to be often difficult to observe by microscopy,[16] it may be determinative for the mechanical properties of the sintered material. Accordingly, considerable effort was invested by the authors in trying to identify a glassy phase in the APS alumina of this study. Both chemical and microscopic analyses, including preliminary TEM investigations, failed to reveal any significant evidence for the presence of such a secondary phase. It is likely, considering the history of the material, and the fast cooling it undergoes from the melt, that a significant portion of the additives which normally help to form a glassy phase remain in solid solution. WDX analysis failed to distinguish any compositional variation across the splats or at the splat interfaces.

3.2 Mechanical and physical testing

The results and standard deviations of the mechanical tests are summarized in Table 1. The bending strength and fracture toughness were measured in three-point bending. The crack resistance curves (R-curves) shown in Fig. 4 were determined with CT-samples and the plateau value, K_R^{max}, for loading normal to splat alignment is presented in the table below. No stable crack growth was observed for loading parallel to splat alignment.

The change of density from 3·12 g/cm^3 for as-sprayed alumina to 3·41 g/cm^3 for the annealed material was accompanied by a volume shrinkage of about 9%.

The strength of the as-sprayed material is about 8·2 MPa for loading parallel to the alignment of the platelets (for samples 5–10). This increases to 22·9 MPa after the heat treatment, an increase of nearly a factor of three. A similar increase is observed in fracture toughness. The K_{Ic} measured for loading parallel to splat alignment in the as-sprayed material is about 0·47 MPa$\sqrt{m}$. This increases to 1·44 MPa$\sqrt{m}$ after heat treatment. The values of both strength and fracture toughness are found to be again significantly higher (three to four times) in the direction normal to the splat alignment for both the as-sprayed and the annealed materials.

For both material conditions, as-sprayed and annealed, loading in the direction parallel to splat

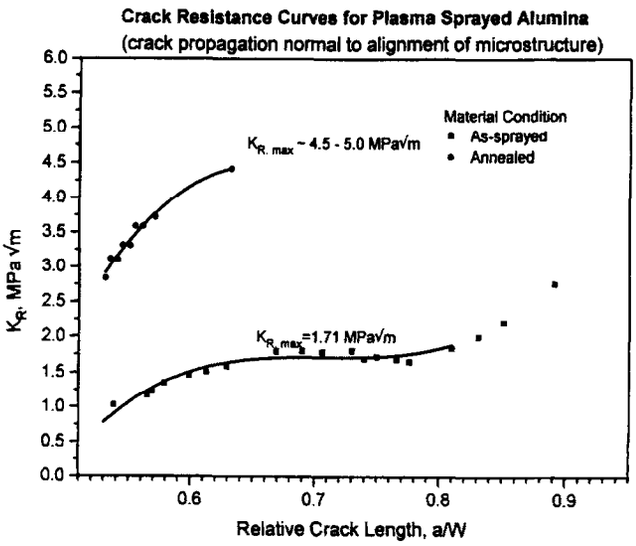

Fig. 4. Crack resistance behaviour of plasma-sprayed alumina.

Table 1. Mechanical and physical properties of plasma-sprayed alumina with respect to loading parallel (‖) and normal (⊥) to splat alignment

Material condition	*Density,* ρ *(g/cm^3)*	*Bending strength,* σ ‖ *(MPa)*	*Bending strength,* σ ⊥ *(MPa)*	*Fracture toughness,* K_{Ic} ‖ *MPa$\sqrt{m}$*	*Fracture* toughness, K_{Ic} ⊥ *MPa$\sqrt{m}$*	*Max. crack* resistance, K_R^{max} ⊥ *MPa$\sqrt{m}$*
As-sprayed	3·12±0·02	8·2±1·3	25·2±1·7	0·47±0·03	1·62±0·15	1·71
Annealed	3·41±0·02	22·9±6·0	63·6±8·6	1·44±0·20	4·64±0·26	4·5

alignment tended to result in catastrophic fracture and largely involved delamination along splat interfaces (Fig. 5(a)). The result was a relatively smooth fracture surface. Loading, however, in the direction normal to the splat alignment led to extensive stable crack growth and crack path deflection before failure. In the as-sprayed condition in particular, the crack path was characteristically transgranular and observation of the fracture surface revealed a very high density of broken (apparent) crack bridges and pulled-out grains (Fig. 5(b)). Crack deflection and delamination become considerably more pronounced after the heat treatment. Interestingly, many more spherical grains (probably incompletely melted powder particles) could be observed on the fracture surface of the heat treated material than had been seen on the fracture surface of the as-sprayed material. The annealed material exhibited mixed transgranular and intergranular fracture, although the contribution of intergranular fracture was considerably increased.

As an undesirable effect of the delamination process two of the annealed CT R-curve specimens failed spontaneously on loading by delamination along the splat interfaces. The crack tended to veer away from the notch direction at a very early stage. One specimen failed completely in the first load cycle and another in the fourth. It was only possible to achieve a reasonable amount of stable crack growth in the desired direction in one heat treated sample. Although the crack still deviated very strongly, curving out and causing delamination along the layers, it branched to come back to the original direction of growth. However, it was considerably displaced from the original plane of propagation when it eventually reached the free edge of the sample (Fig. 6(a)). The resulting R-curves, calculated using the mode I crack projection method, are presented in Fig. 4. Although the behaviour of the samples is not strictly in accordance with linear elastic fracture mechanics, the mode I crack projection simplification has been shown to provide reasonable accuracy, provided that crack deviation is not too extensive.[17] In Fig. 4, data values are plotted only as far as this condition is met.

(a)

(b)

Fig. 5. Fracture surfaces showing (a) delamination in heat-treated material, (b) rough fracture surface (apparent crack bridges) in as-sprayed material.

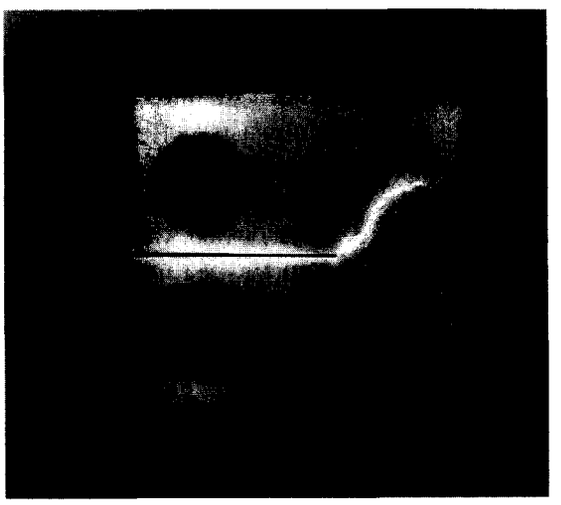

(a)

(b)

Fig. 6. Crack paths in CT fracture toughness samples: (a) in the annealed material, (b) in the as-sprayed material.

In the as-sprayed CT R-curve specimen the crack propagated stably and in the direction normal to loading, as was desired. The crack path was primarily straight with only slight deviations and branching (relative to the heat treated sample) (Fig. 6(b)). The crack path was primarily transgranular. The resulting R-curve is also presented in Fig. 4.

Unfortunately, due to the many large pores it was not possible to detect the very beginning of crack growth in these in-situ tests, so the initial values of K_R presented correspond to K_R values after approximately 1 mm of crack growth. At this point the K_R curves are already highly developed. For both the as-sprayed and the annealed material conditions, since the K_R plateau value is approximately equal to the corresponding fracture toughness values from the three-point bend tests, it may be assumed that any process zone was fully developed before complete fracture even in those tests. In fact, from the R-curves it can be seen that the maximum toughness is reached after crack extension of about 5 to 6 mm.

3.3 Phase and texture analyses

X-ray diffraction results showed that although the starting powder is almost pure α-alumina, the as-sprayed material consists of a mixture of γ-alumina and α-alumina. (In fact some δ-alumina, an intermediate transition phase, found in previous studies[18,19] to occur when the splat cooling rate is too low to retain the γ-alumina phase, e.g. when the deposition substrate has been heated, was also identified on the traces. However, since the intensity measured was so low this phase has been largely ignored in the following analyses of the results). It should be noted that the relative intensity measured for the γ (111) peak in the as-sprayed material was exceptionally low. Nevertheless, the results of the pole figure measurement indicated no obvious crystallographic texture in the as-sprayed material. The γ-alumina is transformed completely to α-alumina during the subsequent heat treatment.

Since no obvious textural effects were observed, the X-ray traces have been used to make a crude quantitative estimate of the phase composition of the as-sprayed material. Assuming that the integrated intensity under a given peak (*hkl*) in the trace of the annealed sample gave the value for 100% α-alumina, the fraction of α-alumina in the as-sprayed material, $F_\alpha^{(hkl)}$, may be estimated by the relationship

$$F_\alpha^{(hkl)} = \frac{[I^{(hkl)}_{\text{as-sprayed}}]}{[I^{(hkl)}_{\text{annealed}}]}, \qquad (3)$$

where $[I^{(hkl)}]$ is the integral intensity under the peak (*hkl*). Since this method is very crude, the values were averaged over a number of isolated peaks in a given trace. To account for system errors, the traces from both the Siemens D500 and the Seifert C3000 diffractometers were used. The results of these analyses are summarized in Table 2. The as-sprayed material was found to consist of approximately 65% metastable γ-alumina.

Table 2. Quantitative X-ray phase analysis of as-sprayed material

α (*hkl*)	*Fraction of* α*-alumina,* $F_\alpha^{(hkl)}$	
	Siemens D500	*Seifert C3000*
(012)	0·28	0·40
(104)	0·31	0·48
(113)	0·32	—
(024)	0·32	0·28
(116)	0·34	0·42
Average	0·314	0·395
Mean value	$F_\alpha \approx 0{\cdot}35$	
Total fraction of γ-alumina $(1 - f_\alpha)$	$F_\gamma \approx 0{\cdot}65$	

4 Discussion

If the annealed material is considered to be completely α-alumina, then the measured density corresponds to a porosity of about 13·7%. If it is assumed that the as-sprayed material contains 65% γ-alumina, then a rule of mixtures calculation (with $\rho_\gamma = 3{\cdot}55$ g/cm^3 and $\rho_\alpha = 3{\cdot}95$ g/cm^3)[20] yields a theoretical density of 3·69 g/cm^3. The measured density of the as-sprayed material then corresponds to a porosity of about 15·4%. Hence, the porosity change on annealing is only 1·7%. This is in contrast to the previously reported change of 5·3% in a similar alumina material after a similar heat treatment.[7] If the volume change of phase transformation only is considered a volume shrinkage of about 7% could be expected, corresponding to a linear shrinkage of about 2·4% for an isotropic material. This agrees well with the 9% volume shrinkage observed.

It becomes clear from the micrographs in Figs 2 and 3 that the critical change in the microstructure that occurs on annealing is not a global sintering of the splats and reduction of overall porosity, but rather a healing of the fine splat-internal defect sub-structure in the as-sprayed material, together with the growing together of some of the finer splat interfaces. Although this healing is obviously not complete, it is sufficiently advanced to result in the change of fracture path and, hence, is responsible for the large increase in strength and fracture toughness.

The mechanism of fracture, for both material conditions, is contrary to that previously reported

for similar coating materials;[21–24] the fracture path of the as-sprayed material is largely through the splats and that of the annealed material largely involves decohesion between the splats. The corresponding fracture toughness values, however, are ranked contrary to expectation, and that for the as-sprayed material is far too low for a true transgranular mode of crack propagation involving the breaking of splats. It is suggested then, that a fine defect structure exists in the splats, which affords the advancing crack an easy, low-energy path. After annealing, access to these fine, pre-existing potential crack paths may be denied to the advancing crack because the defect edges (at least) might have healed. Consequently the crack is forced to advance between the relatively weakly adhering splat interfaces.

In fact, the existence of fine internal substructures within individual splats has been previously observed in plasma-sprayed metal and ceramic coatings. A number of factors can result in such a sub-structure: directional solidification can lead to a fine columnar grain structure with impingement zones containing a high defect density at their interfaces;[25,26] in multi-phase and single-phase bodies differential thermal expansivity and differential cooling rates can lead to microcracking;[21] and if the processing parameters are such that the molten particle can begin to solidify before impact, then the impact on the substrate will cause a high internal microcrack density.[27,28] The fractured splats on the fracture surface of the as-sprayed material seem to be indicative of a columnar internal structure. The cores of some of the splats indicate that they were not properly melted before deposition and the relatively high porosity and weak interfacial bonding suggest that those particles that were molten began to solidify before impact.

Whatever the reason for the material to contain a fine microdefect, microcrack network, it is reasonable to assume that in the as-sprayed material some such sub-structure really does exist. On external loading, this network of fine microcracks provides a naturally weak crack path, which does not allow the formation of a fully effective bridging process zone. This is confirmed by the rather flat *R*-curve observed and the low plateau value of K_R (K_R^{max}= 1·71 MPa$\sqrt{m}$). Nevertheless, the fracture surface still looks as though much grain pull out and crack bridging has taken place. This is shown schematically in Fig. 7(a)).

The model of the splat sub-structure also provides an explanation for the fracture behaviour of the heat treated samples. The heat treatment at a temperature close to the sintering temperature of alumina results in recrystallization and the healing (growing together) of much of the fine crack substructure, or defect structure. A crack then follows the next path of least resistance, i.e. the crack propagates between the open interfaces and attempts to circumvent the elongated splats (Fig. 7(b)). Spherical inclusions in the crack path provide pivotal points for the crack to deflect into another plane of propagation; hence these particles are found easily and frequently on the fracture surface. Failure occurs primarily by intergranular delamination. Extensive crack path deflection and true crack bridging and hinging is then effective, leading to considerable increases in strength and toughness. A very sharply rising *R*-curve with a high plateau value is the result.

The significance of the suggested model is that the highly anisotropic layering of the microstructure is not always critical in determining the properties of the plasma-sprayed ceramic body, but rather the splat-internal structure. For instance, the fine defect structure would increase the local

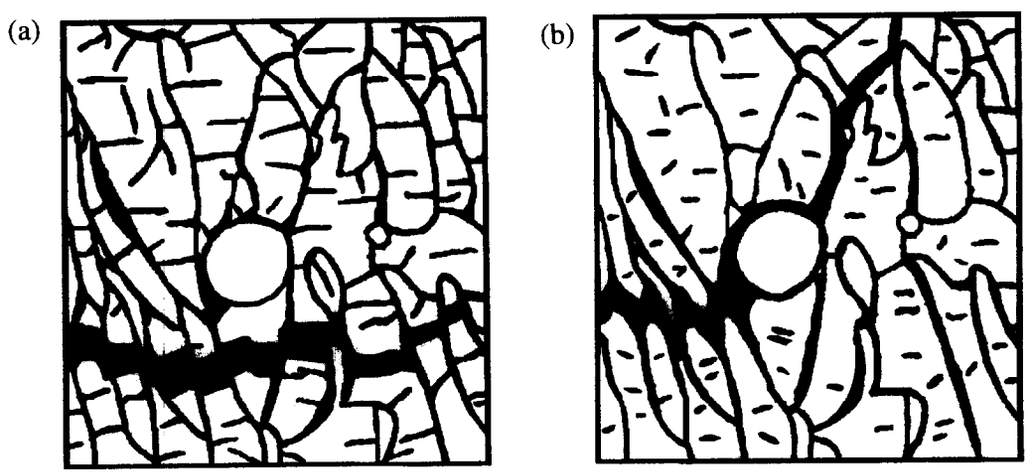

Fig. 7. Schematic representation of (a) transgranular crack advance through pre-existing microcrack sub-structure in as-sprayed material, (b) forced crack deviation around splats leading to extensive crack deflection (microcracks have partially healed on annealing).

compliance of the microstructure, allowing it to accommodate thermal straining more easily and leading to exceptionally good thermal shock resistance. However, service at temperatures where diffusion processes are activated and the defects can begin to heal will result in a significant loss in thermal shock resistance, despite the corresponding increase in fracture toughness. In fact, this behaviour is exactly what has been previously reported for similar materials where ΔT_{max} drops from over 1000°C for a material in the as-sprayed condition to about 750°C for an annealed material.[6] Since the impeding of internal diffusion at elevated temperature is exceptionally difficult, this deterioration in thermal shock resistance is almost inevitable.

The strength and fracture toughness behaviour observed for a fracture path parallel to splat alignment may be assumed to follow from similar material behaviour as discussed above. The lower absolute values are obviously a consequence of the greater availability of low-energy fracture paths.

5 Conclusions

It is obvious that the strength and fracture anisotropy exhibited by the investigated plasma-sprayed alumina material is a direct consequence of two separate features: the highly anisotropic alignment of its microstructure and the occurrence in the as-sprayed state of a fine splat-internal defect sub-structure.

For the as-sprayed material the values of strength and fracture toughness vary from poor to acceptable for a high porosity material, depending on the alignment of the microstructure. If the degree of apparent interlocking, crack bridging and grain pull out observed on the fracture surface (for fracture normal to splat alignment) is considered, much higher values might have been expected. However, these well known indications of process zone formation and energy dissipation are misleading. The fracture path observed contradicts that observed in other plasma-sprayed ceramics, being primarily transgranular (i.e. through the splats) instead of along splat interfaces. The weak points in the as-sprayed microstructure are obviously the microcracked splats themselves and not the weak interfaces between the layers.

Annealing the as-sprayed material at a temperature close to the sintering temperature results in a 9% volume shrinkage, largely resulting from the phase change of γ-alumina to α-alumina. There is only a small reduction in overall porosity. Nevertheless, both the strength and toughness increase by about a factor of three. This exceptional rise after heat treatment is largely due to the healing of a microcrack sub-structure which is prevalent in the as-sprayed material condition. Microcrack healing results in the change in crack path from primarily transgranular for the as-sprayed material to primarily intergranular for heat treated material. It is also responsible for the considerable steepening of the *R*-curve of the annealed material. However, the microcrack healing may reduce the ability of the material to accommodate internal thermal stresses and hence be the cause of the reported decrease in the thermal shock resistance.

Strength and fracture toughness for both as-sprayed and heat treated materials in the direction normal to splat alignment are approximately 3·5 to 4 times higher than in the direction parallel to splat alignment. This may partly be attributed to the contribution of real toughening mechanisms such as, for example, crack bridging and deflection for a crack propagating normal to the splat alignment, but also to the relative increase in the amount of material and interparticulate bonds that such a crack must pass through and break.

Acknowledgements

Thanks are due to M. Lengauer for section preparation, to B. Ortner for support in diffractometry and to R. Danzer for useful discussion.

References

1. Smith, R. W. and Novak, R.. Advances and applications in U.S. thermal spray technology I: Technology and materials. *Powder Metallurgy International*, 1991, **23**, 147–155.
2. Smith, R. W., Advancing thermal spray technologies through international collaborative R&D. *Powder Metallurgy International*, 1993, **25**, 78–82.
3. Eschnauer, H. and Lugscheider, E., Fortschritte beim thermischen Spritzen. *Metall*, 1991, **45**, 458–466.
4. Lugscheider, E., Eschnauer, H., Müller, U. and Weber, Th., Quo vadis, thermal spray technology. *Powder Metallugy International*, 1991, **23**, 33–39.
5. Lutz, E. H., Plasma spraying of ceramics — an alternative to conventional production of components. *Interceram*, 1993, **42**, 160.
6. Lutz, E. H., Plasmakeramik. In *Technische Keramische Werkstoffe*, ed. J. Kriegesmann. Deutscher Wirtschaftsdienst, Köln, 1993, Kap 3.4.9.1.
7. Lutz, E. H., Microstructure and properties of plasma ceramics, *J. Am. Ceram. Soc.*, 1994, **77**, 1274–1280.
8. Pawlowski, L., *The Science and Engineering of Thermal Spray Coatings*. Wiley, Chichester, 1995.
9. Glitzen, W. (ed.); *Alumina as a Ceramic Material*. Special Publ. No. 4, The American Ceramic Society, Westerville, OH, 1970.
10. Lutz, E. H. and Florian, R., Schweißen von Plasmakeramik. *Keramische Zeitschrift*, 1993, **45**, 458–460.
11. Swain M. V., *R*-Curve behaviour of magnesia-partially-stabilized zirconia and its significance for thermal shock.

In *Fracture Mechanics of Ceramics, Vol. 6*, eds R. C. Bradt *et al.* Plenum Press, New York, 1983, pp. 345–359.
12. Lutz, E. H. and Swain, M. V., Interrelation between flaw resistance, *R*-curve behaviour and thermal shock strength degradation in ceramics, *J. Am. Ceram. Soc.*, 1991, **74**, 2859–2868.
13. Brown, W. F. and Strawley, J. E., Plane strain crack toughness testing. In *ASTM STP No. 410*, American Society for Testing and Materials, Philadelphia, PA, 1981, pp. 13–15.
14. *Annual Book of ASTM Standards, Vol. 10,* ASTM Designation E 399-81. American Society for Testing and Materials, Philadelphia, PA, 1981.
15. Morrell, R., *Handbook of Properties of Technical & Engineering Ceramics, Part 2: Data Reviews, Section 1: High-Alumina Ceramics.* HMSO, London, 1987.
16. Morrell, R., *Handbook of Properties of Technical and Engineering Ceramics, Part 1. An Introduction for the Engineer and Designer.* HMSO, London, 1989.
17. Fischer, F. D. and Rammerstorfer, F. G., Mode-I Crack projection procedure using the strain energy density criterion. *Theoretical and Applied Fracture Mechanics*, 1994, **20**, 67–74.
18. Eichhorn, F., Metzler, J. and Eysel, W., Röntgenbeugungsuntersuchungen an plasmagespritzten Aluminiumoxidschichten. *Metalloberfläche Angew. Elektrochemie*, 1972, **26**, 212–213.
19. McPherson, R., Formation of metastable phases in flame and plasma-prepared alumina. *J. Mater. Sci.*, 1973, **8**, 851–858.
20. Huffadine, J. B. and Hollands, E. J., *Flame Spraying of Ceramic Materials.* Plessey Co. Ltd., Brit. Patent 903, 709, 1962.
21. Harmsworth, P. D. and Stevens, R., Microstructure of zirconia–yttria plasma-sprayed thermal barrier coatings. *J. Mater. Sci.*, 1992, **27**, 616–624.
22. Siemers, P. and Mehan, R. L., Mechanical and physical properties of plasma sprayed stabilized zirconia. *Ceramic Engineering and Science Proceedings*, 1983, **3**, 828–840.
23. LaPierre, K., Herman, H. and Tobin, A. G., The microstructure and properties of plasma sprayed ceramic composites. *Ceramics Engineering Science Proceedings*, 1991, **12**, 1201–1221.
24. Safai, S., A microstructural investigation of plasma-sprayed metal and oxide coatings. Ph.D. Thesis, State University of New York at Stony Brook, 1979.
25. Safai, S. and Herman, H., Plasma-sprayed materials. *Treatise on Materials Science and Technology, vol. 20*, Academic Press, New York, 1981, pp. 183–213.
26. Braue, W. *et al.*, In-plane microstructure of plasma-sprayed Mg-Al spinel and 2/1-mullite based protective coatings: An electron microscopy study. *J. Eur. Ceram. Soc.*, 1996, **16**, 85–97.
27. Houben, J. M. Relation of the adhesion of plasma sprayed coatings to the process parameters size, velocity and heat content of the spray particles. Ph. D. Thesis, Technical University of Eindhoven, Holland, 1988.
28. Sampath, S. and Herman, H., Microstructural development of plasma sprayed coatings. *12th International Thermal Spraying Conference, London*, 1989, Paper 53.